

# DIFFRACTION SIMULATIONS OF THE LCLS FEL PULSE ON CRYSTALS

S. Reiche, UCLA, Los Angeles, CA 90095, USA

## Abstract

The Linac Coherent Light Source operates as a Self-Amplified Spontaneous Emission Free-Electron Laser (SASE FEL), where transverse coherence is achieved by the domination of the FEL Eigenmode with the largest growth rate. However complete transverse coherence is not guaranteed because there are multiple eigenmodes with similar growth rates for a low-diffracting FEL, such as the LCLS. In addition the mode purity can be degraded by collective electron beam motion.

In this paper the transverse coherence for the LCLS pulse is investigated with respect to scattering on crystals. The degradation in the contrast and size of the Bragg peaks is analyzed for a step wise improved modeling of the experiment (steady-state, time-dependent and start-end simulations). The impact on diffraction experiments, including the proposed experiment to measure the transverse coherence, is discussed.

## INTRODUCTION

Free-electron Lasers (FEL) allow for tunability of the resonant wavelength [1] in contrast to quantum lasers where the wavelength is defined by the energy difference of the two electron states in the lasing medium. The concept of FELs can also be extended to shorter wavelength towards the X-regime by starting from the spontaneous radiation as its own seed [2]. The gain per single pass is high enough to reach saturation and thus to eliminate the restriction of an enclosing optical cavity. Several of these Self-amplified Spontaneous Radiation (SASE) FELs have been successfully operated [3] with succeeding shorter wavelengths leading up to X-ray FELs such as LCLS [4] and the European XFEL, currently under construction or preparation.

In a SASE FEL coherence is build up during the amplification process [5]. The phase information of the radiation field and bunching is propagated in the longitudinal direction by the slippage of the radiation field and in the transverse direction by diffraction and the betatron oscillation of the electrons. However for X-ray FELs both methods become less effective and the degree of coherence is limited. Therefore it is essential to measure longitudinal and transverse coherence as basic properties of the FEL pulse. For the longitudinal coherence, measurement methods normally analyze the fluctuation of the radiation power or they take single-shot spectra with sufficient resolution. On the other hand, transverse coherence determines the diffraction

pattern. Either slits or crystals are placed into beam and the distribution of the diffracted radiation is measured by an imaging system. From the reconstruction of the diffraction pattern information on the degree of coherence is obtained.

In this paper we discuss the expected diffraction of the LCLS beam on a crystal, in particular in the context of the transverse and longitudinal coherence of the radiation pulse. As the starting point for these simulations wavefronts have been extracted from steady-state and time-dependent simulation of the LCLS X-ray FEL [6]. The focus is on a possible experimental set-up in the Near Experimental Hall, which becomes accessible during the commissioning and early operation of the FEL.

## NUMERICAL MODELING

The diffraction of radiation by a crystal is complicated to calculate unless some simplifying approximations are used such as full longitudinal and transverse coherence. However this is not the case for the output of the LCLS radiation beam and the diffraction pattern has to be calculated based on first principles. For our discussion we are not interested to derive the location of the Bragg peaks which are well defined by the crystal properties and has no information about the coherence of the incident field. Instead the interest is in the width of each Bragg peak, determined by the crystal size and/or the incident radiation. Therefore the calculation of the distribution is restricted to an arbitrarily chosen Bragg peak.

The diffraction process is broken down into the initial scattering of the radiation field on each atom of the crystal lattice. For the sake of simplicity we assume a cubic cell as the basis of the lattice (e.g. Si with a cell size of 5.44 Å in all dimensions). The emission of the scattered field depends on the explicit structure of the cell and it is expressed by the directivity function  $f(\vec{r})$ , where  $\vec{r} = \vec{R} - \vec{r}_{ijk}$  is the direction vector from the cell position, indicated by the indices  $i, j$  and  $k$  and the point of observation  $\vec{R}$ . Following Huygen's principle each cell emits a spherical wave, weighted by the directivity function  $f$ , with an amplitude proportional to the incident field  $A_i$ . The field observed is then

$$A(\vec{R}, t) = \sum_{i,j,k} A_i(\vec{r}_{ijk}, t) f(\vec{R} - \vec{r}_{ijk}) \frac{e^{ik|\vec{R} - \vec{r}_{ijk}|}}{|\vec{R} - \vec{r}_{ijk}|} e^{i\omega t} \quad (1)$$

We simplify the expression under following assumptions. First, the point of observation  $\vec{R}$  lies far outside of the crystal ( $R \gg r_{ijk}$ ) and that the directivity function is smooth in

$\vec{R}$ . Second, the crystal is aligned to the coordinate system with  $\vec{r}_{ijk} = d(n_i\vec{e}_x + n_j\vec{e}_y + n_k\vec{e}_z)$ . Third the incident radiation field propagates in the  $z$ -direction and the explicitly delay in the emission from the deeper layers of the crystal is expressed by  $i\omega t \equiv ikdn_k$ . Eq. 1 then becomes

$$A(\vec{R}, t) = f(\vec{R}) \frac{e^{ikR}}{R} \sum_{i,j,k} A_i(\vec{r}_{ijk}, t) e^{i\varphi_{ijk}} \quad (2)$$

with the phase

$$\varphi_{ijk} = kd[n_i \sin \phi \sin \theta + n_j \cos \phi \sin \theta + n_k(1 - \cos \theta)] \quad (3)$$

where  $\phi$  and  $\theta$  are the polar and azimuthal angle of the direction of observation, respectively.

To calculate the interference between the spherical waves from each cell the summation has to be done over all sources which arrives at the point of observation at the same time. Due to the finite size of the crystal this summation results in not only a single wavefront of the incident beam contributing to the interference but an extended volume intersecting with the radiation pulse. Fig. 1 shows the geometry of the radiation emitted under the diffraction angle  $\theta$ . Because the path length differs from each corner of the crystal to the interference plane the incident field at  $B'$ , scattered at  $B$ , is interfering with the field  $A'$  from location  $A$  of the crystal. The longitudinal separation between  $A'$  and  $B'$  is  $b(1 - \cos \theta)$ . Similarly, point  $D'$  is ahead of  $B'$  by the distance  $a \sin \theta$ . Only in the forward direction  $\theta = 0$  the interference arises from a single wavefront of the incident radiation. However if the radiation is longitudinally coherent the field values from the indicated volume are identical to a single wavefront as well, which would simplify the calculation of the interference pattern. This is not the case for SASE FELs such as LCLS, which has a longitudinal coherence length of about 300 nm at saturation.

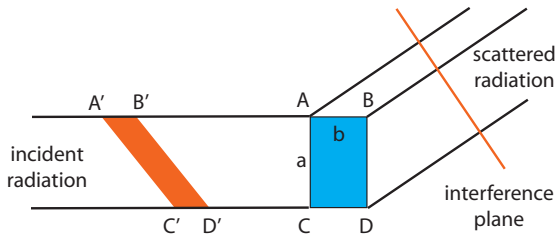


Figure 1: Effective source size (orange area) of incident radiation field to interfere when scattered at a crystal (blue area)

Numerically it is highly inefficient to sum over all grid points individually, because even a volume of  $1 \mu\text{m}^3$  of a Si crystal has about  $6 \cdot 10^9$  cells. In addition the resolution is mainly given by the discretization of the incident radiation field, which is much coarser than the cell size of the crystal. Therefore the incident radiation amplitude can be

kept constant over a sub-domain of the crystal. The effective source size has  $N_x$ ,  $N_y$  and  $N_z$  sampled radiation field point for each dimension, respectively. The sub-domain has therefore the size of  $n_x = a/dN_x$ ,  $n_y = a/dN_y$  and  $n_z = b/dN_z$ . With an arbitrarily numbering of the cells and the corresponding incident radiation field, the summation of Eq. 2 is reduced to

$$A(\vec{R}) = c(\vec{R}) \sum_{j=1}^{N_x N_y N_z} A_i(\vec{r}_j) e^{ik_x x_j} e^{ik_y y_j} e^{i(k-k_z)z} \quad (4)$$

$$\times \frac{1 - e^{in_x k_x d}}{1 - e^{ik_x d}} \cdot \frac{1 - e^{in_y k_y d}}{1 - e^{ik_y d}} \cdot \frac{1 - e^{in_z(k-k_z)d}}{1 - e^{i(k-k_z)d}}$$

with the constant factor

$$c(\vec{R}) = f(\vec{R}) \frac{e^{ikR}}{R}$$

and the vector  $\vec{k}$  of the wavenumber, pointing into the direction of observation. The last three factors of Eq. 4 are independent in the summation and can be calculated in advance. What remains is similar to a 3D Fourier transformation.

## SIMULATION RESULTS

The main purpose of the simulation is to show the difference of the diffraction from a fully coherent source. For that some assumption and approximation have been made, which significantly reduce the computational time. The forward Bragg peak has been selected, ignoring the experimental challenge to separate the diffraction pattern from the bulk of the incident radiation, which is not scattered by the crystal. In addition it avoids the mixing of the transverse and longitudinal field information of the radiation, which would otherwise yield a time-consuming selection of field information of the incident beam. We assume the experimental station to be in the Near Experimental Hall (NEH), 115 m downstream the undulator with an unfocused FEL beam.

### Fundamental Gauss-Hermite Modes

The numerical algorithm is tested with an analytical expression of the radiation field, using a fundamental Gauss-Hermite mode [7]. The mode is fully defined by three parameters: the wavelength, the size of the waist and the position of the waist. The radiation wavelength is kept constant for all runs with a value of  $1.5 \text{ \AA}$ , the resonant wavelength of LCLS.

The first scan is over the waist size  $w_0$  with the waist placed directly at the location of the crystal. The rms diffraction angle depends inversely on the waist size, as shown in the left plot of Fig. 2. This confirms that diffraction on a crystals acts like a spectrometer in the transverse direction (Eq. 4). Therefore it is not surprising that the rms size does not depend on the position  $z_0$  of the waist before the crystal (right plot of Fig. 2), because the diffraction pattern is proportional to the far field distribution of

the Gaussian-Hermite mode which is per definition independent of the waist position.

These results are not representing the diffraction from the LCLS radiation beam, but they allow a good comparison of the following results, based on LCLS simulation, with an equivalent Gauss mode.

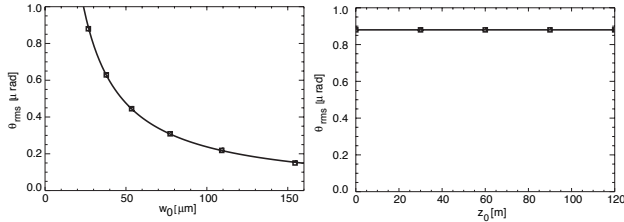


Figure 2: Dependence of the rms size of the Bragg peak on the waist size and position of an fundamental Gauss-Hermite mode as incident radiation field.

### Steady-State Simulation

Steady-state simulations include explicitly longitudinal coherence by a periodic boundary condition of a single slice of the radiation field. However they are restricted to model only FEL amplifiers. To yield the same saturation length as in the SASE case an effective seeding power was chosen of about 5 kW. The point of saturation lies around 100 m, while the simulation covers the entire undulator length of 130 m. The simulated wavefront is then propagated down the optical beam line by 115 m, using Fresnel integration. The full width of the incident radiation is about 500  $\mu\text{m}$  at the location of the crystal, but the distribution (see Fig. 3) is not as smooth as a fundamental Gauss-Hermite mode.

The rms size of the Bragg peak is below 1  $\mu\text{rad}$  and correspond to a waist size of  $w_0 = 28 \mu\text{m}$ , when compared to a Gauss-Hermite. As discussed above, the size of the incident radiation field at the crystal location has no importance because it would forcefully exclude the impact of the phase front curvature on the diffraction process. Instead, the waist size of the FEL beam has to be used, except that the FEL beam never goes through a waist. In the linear regime of the FEL, where gain guiding preserves the profile of the radiation, the wavefront has a residual curvature. At saturation, gain guiding stops and the field diffracts according to free-space propagation. Therefore the ‘virtual’ position of the waist is always before the point of saturation. For FELs in the Ångstrom region diffraction is negligible during the FEL amplification and the curvature of the FEL eigenmode is almost flat. This yields that the virtual waist position is almost identical to the saturation point. The steady-state simulation has a radiation size of less than 29  $\mu\text{m}$  at saturation and is therefore in good agreement with the estimate of  $w_0 = 28 \mu\text{m}$  of the equivalent Gauss-Hermite mode.

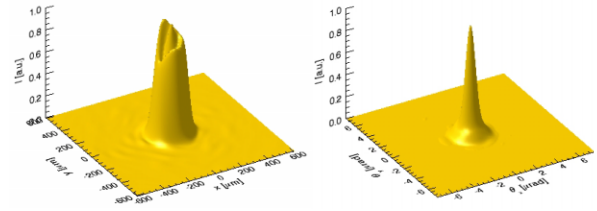


Figure 3: Incident and diffracted field distribution from a steady-state simulation for LCLS.

### Start-End Simulation

Start-end simulations model the entire experiment from the creation of the electron beam with an rf photo-electron gun, the propagation and compression of this beam through the beam line, the injection into the FEL and the transport of the FEL radiation to the experimental station. For X-ray FELs, the bunch is longer than the distance electrons can communicate with each other during the FEL amplification. When started by the initial fluctuation of the electron position in a SASE FEL, parts of the electrons bunch amplifies the radiation independently. The longitudinal coherence is limited to submicron distances and the radiation pulse consists of many spikes. The simulation covers each spike with multiple wavefronts. The diffraction pattern is calculated for each wavefront and the resulting intensity distributions are added up.

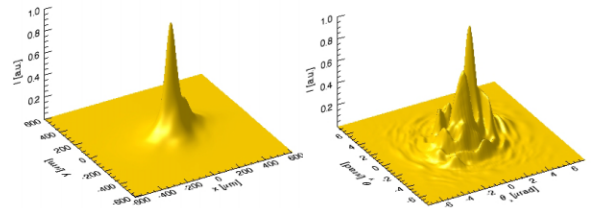


Figure 4: Incident and diffracted field distribution from a time-dependent simulation for LCLS, based on an start-end simulation input deck for the electron beam.

The incident and scattered radiation field is shown in Fig. 4. Compared to the steady-state simulation, the incident field distribution looks smaller but actually has large tails increasing the full size to 850  $\mu\text{m}$ . The Bragg peak is not smooth and has a structure similar to a speckle pattern. The opening angle is 2.6  $\mu\text{rad}$ . Because this number differs significantly to the steady-state result a comparison with an equivalent fundamental Gauss-Hermite mode loses its merits, as it yields an effective waist size of only  $w_0 = 9 \mu\text{m}$ . It would be wrong to identify this number as the effective transverse size of coherence. The systematic error is that the SASE FEL pulse consists of higher order modes. These modes would yield a larger opening angle for the same waist size. Based on the same waist size

the mode  $H_{nm}$  would have a larger opening angle by the factor  $\sqrt{1+n+m}$ . For the results obtained here, it gives approximately  $n, m = 4$ .

The reason for the higher mode content lies in the electron beam, driving the SASE FEL. First, the electron beam is only aligned to the undulator axis as a whole, while any longitudinal slice of the electron distribution may have an initial offset or angle at the undulator entrance. The collective betatron oscillation of each slice sweeps the emission of radiation in the horizontal plane, which then slips ahead in the bunch and interferes with radiation, emitted under an different angle. Second, collective emission effects (coherent synchrotron radiation [8]) within the bunch compression yield a change in the electron energy, depending on the position within the bunch. This energy change is coupled to the transverse position or momentum of the electron if the dispersion function is not zero at the undulator entrance. This correlation causes the emission under an angle and thus the excitation of higher modes. Fig. 5 shows the initial condition of the electron slice centroid at undulator exit and the betatrons oscillation of three slices.

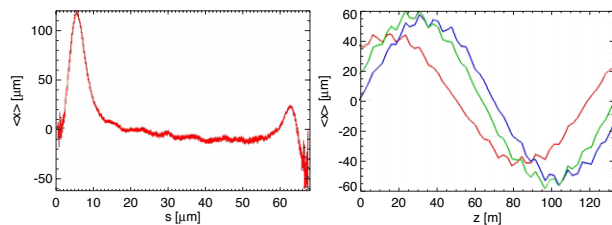


Figure 5: Initial electron slice position at undulator entrance (left plot) and betatron oscillation along undulator for three different slices (right plot, 20, 50 and 62  $\mu\text{m}$  from head for green, blue and red curve, respectively).

## TRANSVERSE AND LONGITUDINAL COHERENCE

The diffraction patterns depend significantly on the coherence of the LCLS pulse. In contrast to crystallography experiments at third generation light sources, where the radiation is selected through a pin hole and a narrow band monochromator to guarantee full coherence, this is not the case for the raw output of an SASE FEL.

The high intensity of the emitted radiation, which is mainly generated by the spontaneous radiation, do not permit to place optical elements in the beam line to focus the beam down. Instead the FEL beam diffracts naturally till it has a size of about 0.5 mm at the Near Experimental Hall, which is located 115 m downstream the undulator. To probe for full transverse coherence a mono-crystal has to be match to that size. Alternatively slits have to be aligned to each other with Ångstrom precision.

Experimentally it is very hard to extract the Bragg peak in the forward direction, because it is covered by the inci-

dent beam, which is not deflected by the scattering on the crystal. For the example of a Si crystal and a transverse extension of about 1 mm, the opening angle of the forward Bragg Peak is around 1  $\mu\text{rad}$ , which is comparable to the natural divergence of the FEL beam. Thus the Bragg peak will always be lying within the cone of the FEL radiation.

Using off-axis Bragg peaks introduce a mixing of longitudinal and transverse coherence. With a longitudinal coherence of about 350 nm and a transverse extend of 500  $\mu\text{m}$  it requires only a deflection angle 0.7 mrad or more to mix the phase information of two adjacent spikes. However for Si the smallest deflection angle is three orders of magnitude larger. Therefore it seems that crystals are general unsuitable for measurement of the transverse coherence for LCLS and that slits with a spacing of around 1  $\mu\text{m}$  or below are favorable. Alternatively the FEL beam can be focused down, but that would require that the measurement is moved to the Far Experimental Hall.

## CONCLUSION

With the improvement in the start-end modeling process of the LCLS X-ray, the propagation of the FEL output pulse towards the experimental station has been included and used to simulate a generic experiment, where the radiation is scattered at a Si crystal.

With respect to the ideal performance of LCLS the resulting pulse acts similar to a fundamental Gauss-Hermite mode with a matched to the mode size at the point of saturation. However slight perturbations (e.g. centroid mismatch or energy correlation with the transverse position and/or momentum) alter the diffraction performance; Main reason is that these perturbations couple to higher modes which then increase the rms size of the diffraction pattern.

Another problem is the limited longitudinal coherence, in particular when the transverse size is large. Therefore crystals are less suitable than slit masks, because radiation tends to scatter under a larger angle and thus enhances the impact of the longitudinal coherence.

## REFERENCES

- [1] J.M.J. Madey, *J. App. Phys.* **42** (1971) 1906
- [2] R. Bonofacio *et al*, *Opt. Comm.* **50** (1984) 373
- [3] A list can be found e.g. W.B. Colson, *Proc. of the FEL 2004 Conference* (2004) 706
- [4] *LCLS CDR*, SLAC Report No. SLAC-R-593, 2002
- [5] S. Krinsky and L.H. Yu, *Phys. Rev.* **A35** (1987) 3406
- [6] S. Reiche *et al*, *Bucl. Inst. & Meth.* **A483** (2002) 70
- [7] A.E. Siegman, *Lasers* (University Science Book, Mill Valley, CA, 1986)
- [8] Y.S. Derbenev *et al*, TESLA-FEL 95-05, DESY, Hamburg, Germany (1995)